IOP Publishing Plasma Sources Science and Technology
Plasma Sources Sci. Technol. 26 (2017) 085006 (13pp) https://doi.org/10.1088/1361-6595/aa7c88

The effect of realistic heavy particle induced secondary electron emission coefficients on the electron power absorption dynamics in single- and dual-frequency capacitively coupled plasmas

M Daksha[1,2], A Derzsi[1,3], S Wilczek[4], J Trieschmann[4], T Mussenbrock[5], P Awakowicz[2], Z Donkó[3] and J Schulze[1,2]

[1] Department of Physics, West Virginia University, Morgantown, WV 26506, United States of America
[2] Institute of Electrical Engineering and Plasma Technology, Ruhr-University Bochum, D-44780 Bochum, Germany
[3] Institute for Solid State Physics and Optics, Wigner Research Centre for Physics, Hungarian Academy of Sciences, 1121 Budapest, Konkoly Thege Miklós str. 29-33, Hungary
[4] Institute of Theoretical Electrical Engineering, Ruhr-University Bochum, D-44780 Bochum, Germany
[5] Brandenburg University of Technology, Cottbus-Senftenberg, Siemens-Halske-Ring 14, D-03046 Cottbus, Germany

E-mail: manudaksha@gmail.com)

Received 11 May 2017, revised 20 June 2017
Accepted for publication 29 June 2017
Published 27 July 2017

Abstract

In particle-in-cell/Monte Carlo collisions (PIC/MCC) simulations of capacitively coupled plasmas (CCPs), the plasma-surface interaction is generally described by a simple model in which a constant secondary electron emission coefficient (SEEC) is assumed for ions bombarding the electrodes. In most PIC/MCC studies of CCPs, this coefficient is set to $\gamma = 0.1$, independent of the energy of the incident particle, the electrode material, and the surface conditions. Here, the effects of implementing energy-dependent secondary electron yields for ions, fast neutrals, and taking surface conditions into account in PIC/MCC simulations is investigated. Simulations are performed using self-consistently calculated effective SEECs, γ^*, for 'clean' (e.g., heavily sputtered) and 'dirty' (e.g., oxidized) metal surfaces in single- and dual-frequency discharges in argon and the results are compared to those obtained by assuming a constant secondary electron yield of $\gamma = 0.1$ for ions. In single-frequency (13.56 MHz) discharges operated under conditions of low heavy particle energies at the electrodes, the pressure and voltage at which the transition between the α- and γ-mode electron power absorption occurs are found to strongly depend on the surface conditions. For 'dirty' surfaces, the discharge operates in α-mode for all conditions investigated due to a low effective SEEC. In classical dual-frequency (1.937 MHz + 27.12 MHz) discharges γ^* significantly increases with increasing low-frequency voltage amplitude, V_{LF}, for dirty surfaces. This is due to the effect of V_{LF} on the heavy particle energies at the electrodes, which negatively influences the quality of the separate control of ion properties at the electrodes. The new results on the separate control of ion properties in such discharges indicate significant differences compared to previous results obtained with different constant values of γ.

Keywords: capacitively coupled plasmas, plasma-surface interaction, secondary electron emission

1. Introduction

Low-pressure capacitively coupled plasmas (CCPs) are widely used in the manufacturing of high-tech devices. They play a pivotal role in a variety of technological processes such as surface etching, deposition and sputtering [1–3]. These applications are based on the interaction of plasma particles with the electrode surfaces: the plasma changes the nature of the surface exposed to particle bombardment. In turn, the surface also plays an important role in changing the nature of the plasma via various surface processes (e.g., particle absorption, reflection, emission).

The particle-in-cell (PIC) approach combined with Monte Carlo type treatment of collision processes (PIC/MCC method) is a powerful self-consistent numerical technique for the kinetic description of low-pressure CCPs [4–10]. In PIC/MCC models of such discharges several assumptions are typically made regarding the description of the plasma-surface interaction. For instance, the emission of secondary electrons from electrode surfaces is assumed to be induced solely by positive ions, the contribution of other plasma species to this process is generally neglected. Further, the secondary electron emission coefficient (SEEC), γ, is assumed to be constant (typically guessed to be 0.1 in most studies) as is the electron reflection coefficient (fixed at 0.2 in most studies), independent of the incident particle energy and angle, the electrode material and its surface conditions. These simplifications are made mainly due to the lack of reliable data on surface processes for various combinations of the discharge gas and electrode material (with different surface properties). However, the above mentioned simplifications are commonly encountered even in computational studies of those discharges for which experimental or theoretical data on specific surface processes are available in the literature [11–16].

The assumptions related to the description of plasma-surface processes in kinetic models of CCPs have a strong effect on the calculated discharge characteristics [17–24]. The ion induced SEEC, γ, which is usually an input parameter in PIC/MCC simulations of CCPs and is kept constant independent of the energy of the incident particle, electrode material and surface conditions, was found to strongly influence the electron power absorption and ionization dynamics (i.e., the discharge operation mode). Increasing the value of the ion induced SEEC was found to result in a transition of the discharge operation mode from the α-mode [25–32], where ionization by electrons accelerated by the expanding sheaths dominates (α-mechanism), to the γ-mode [25, 33–38], where ionization due to secondary electrons accelerated and efficiently multiplied collisionally in the sheaths is the main ionization mechanism (γ-mechanism). Besides influencing the plasma density, the sheath width, and other plasma parameters, the value of the (constant) SEEC can also largely affect the realization of the separate control of ion properties at the electrodes in dual-frequency CCPs [33, 34, 39–41]. Due to these effects, a realistic implementation of the secondary electron emission process in PIC/MCC models of CCPs is essential [17].

The contribution of fast neutrals, metastable atoms, and VUV photons to secondary electron emission at the electrode surfaces can also be significant [11]. Phelps and Petrović have shown that the secondary electron yields due to these species largely depend on the discharge conditions and properties of the electrode surface [11]. The effect of all the different species can be taken into account in discharge models by using an 'apparent' or 'effective' SEEC, γ^* [11]. This γ^* coefficient, defined as the ratio of the secondary electron flux to the ion flux at the electrode, has previously been obtained for a homogeneous electric field [11] and for cathode fall conditions in abnormal DC glow discharges [42–44] in argon. In order to describe the secondary electron emission process more realistically in PIC/MCC models of CCPs, such γ^* coefficients, as well as SEECs determined *in situ* by computationally assisted spectroscopic techniques [45] can be used.

The importance of a precise description of the secondary electron emission process, taking into account the particle energies and surface conditions, has previously been pointed out for analytical glow discharges [46, 47] as well as in a few studies of low-pressure CCPs [17, 19–21] in argon. These studies have shown that, depending on the discharge conditions, fast neutrals can also play an essential role in processes taking place both in the discharge volume and at the electrode surfaces. In [17] it was demonstrated that fast neutrals affect the ionization directly via gas-phase collisions and indirectly by generating electrons inside the sheaths and at the electrodes (this leads to an increase of the effective SEEC); these effects were found to be most important at low (5 Pa) and intermediate (20 Pa) gas pressures. This study also points out that assuming a constant value of the SEEC and tracing only ions in the simulations results in an unrealistic description of the discharge physics. However, in [17], only 'dirty' electrodes were considered (i.e., the surface conditions were not varied). Details of the mode transition induced by assuming different surface conditions and the effects of using realistic SEECs in PIC/MCC simulations of dual-frequency CCPs were not studied.

Here, we investigate the effects of using realistic energy-dependent SEECs and taking into account the properties of the electrode surfaces on the calculated plasma parameters in PIC/MCC simulations of low-pressure single- and dual-frequency CCPs in argon. Simulations are performed by assuming 'clean' metal surfaces as well as 'dirty' electrodes in the model, while the effective SEECs, γ^*, corresponding to these surface conditions are calculated self-consistently. 'Dirty' electrodes represent surfaces treated by using the standard chemical and mechanical cleaning procedures (typical laboratory conditions, e.g., oxidized or contaminated samples), while 'clean' electrodes correspond to atomically clean surface conditions (e.g., samples heavily sputtered by

ion bombardment in high vacuum environment) [11]. The energy-dependent secondary electron yields for heavy particles are obtained according to formulae given in [11, 48]. The results of the simulations for 'dirty' and 'clean' electrode surfaces are compared to those obtained by using a constant ion induced SEEC $\gamma = 0.1$ in the calculations. In single-frequency discharges driven at $f = 13.56$ MHz, simulations are performed at different pressures between 10 and 130 Pa for three different voltage amplitudes and the transition of the discharge operation mode between the α-mode and the γ-mode is studied. We find that the pressure at which the transition between these modes is observed strongly depends on the surface conditions: for 'clean' metal surfaces the transition takes place at a higher pressure compared to the case of $\gamma = 0.1$, while for 'dirty' metal surfaces, the discharge operates in α-mode for all conditions investigated. The source of these differences is the different value of γ^* obtained from the calculations for 'dirty' and 'clean' surface conditions, which are different also from 0.1. In classical dual-frequency discharges [49–51], driven by two significantly different frequencies (1.937 MHz + 27.12 MHz), simulations are performed at 6.6 Pa for different values of the low-frequency voltage amplitude (taking values between 0 and 685 V, at a constant high-frequency voltage amplitude of 200 V). The separate control of the mean ion energy and ion flux at the electrodes is analyzed for different surface conditions. The discharge conditions are similar to those previously studied by using different (constant) secondary electron yields for ions in PIC/MCC simulations of classical dual-frequency discharges [33, 34]. Now, we find that the results differ from those obtained for constant values of γ, since the effective SEEC γ^* depends on the discharge operating conditions. For 'dirty' surfaces, γ^* significantly increases with increasing low-frequency voltage amplitude, V_{LF}, which negatively influences the quality of the separate control of ion properties at the electrodes.

In section 2, we describe the PIC/MCC model and specify the discharge conditions investigated. The results are presented in section 3, which is split into two parts: first, the effect of the surface conditions on the electron power absorption and ionization dynamics is investigated in single-frequency discharges. Second, the effect of the surface conditions on the ionization dynamics and the separate control of ion properties at the electrodes is investigated in classical dual-frequency discharges. Conclusions are drawn in section 4.

2. Simulation setup

The simulations are performed by using our electrostatic PIC code complemented with Monte Carlo treatment of collision processes (PIC/MCC) [17, 52, 53]. This approach is fully capable of accounting for non-equilibrium kinetic effects in low temperature plasmas [54–57]. The code is one-dimensional in space and three-dimensional in velocity space, thus it is suitable to describe geometrically symmetric CCPs. The plane, parallel, and infinite electrodes are separated by a distance of $d = 2.5$ cm. The discharge gas is argon, the gas temperature is constant, taken to be 350 K. We assume that the electrodes are made of the same material with identical surface conditions. The electron reflection probability is set to 0.2 for all conditions [58].

The plasma particles traced in the simulations are electrons, Ar^+ ions and fast Ar atoms (Ar^f). The atoms of the background gas with kinetic energy above the threshold value of 23 eV are considered here as fast atoms. This energy value is near the threshold energy for the excitation of Ar atoms by fast neutrals [17]. The fast neutrals are traced in the simulations until their energy becomes lower than the threshold value, or until they reach one of the electrodes.

In the simulations different approaches are used to describe the secondary electron emission process at the electrodes: self-consistently calculated effective SEEC, γ^*, and constant SEEC, γ (taking the value typically used in PIC/MCC simulations of CCPs, $\gamma = 0.1$).

The effective SEEC, γ^*, is calculated by following the concept of Phelps and Petrović [11]:

$$\gamma^* = \frac{\sum_{k=1}^{N_i}\gamma_i(\epsilon_k) + \sum_{k=1}^{N_a}\gamma_a(\epsilon_k)}{N_i}, \quad (1)$$

where ϵ_k is the energy of the kth ion or atom (upon arrival at the electrode). γ_i and γ_a are the energy-dependent secondary electron yields for ions and fast atoms, respectively. N_i and N_a are the total number of ions and fast atoms reaching a given electrode during an RF period. This coefficient, by definition, corresponds to the number of electrons emitted per ion reaching the electrode, while other plasma particles can also contribute to the emission of secondary electrons. This is why only N_i appears in the denominator of equation (1). Under the conditions investigated, mainly ions and fast neutrals contribute to secondary electron emission. Therefore, the contribution of other plasma species is neglected in the numerator of equation (1). We note that γ^* obtained via this definition, can differ significantly for different physical settings (homogeneous electric fields conditions [11], DC cathode fall conditions [42, 43], and RF discharges), due to the specific particle dynamics and electric field distributions, even when the same gas-electrode material combination is considered [17].

We perform simulations assuming 'dirty' metal electrodes and 'clean' metal electrodes. γ_i and γ_a are calculated according to formulas given in [11, 48]. For 'dirty' surfaces formulas, B15 and B17 in [11] are used (a correction to B15 is given in [48]):

$$\gamma_i(\epsilon) = \frac{0.006\epsilon}{1 + (\epsilon/10)} + \frac{1.05 \times 10^{-4}(\epsilon - 80)^{1.2}}{(1 + \epsilon/8000)^{1.5}}, \quad (2)$$

$$\gamma_a(\epsilon) = \frac{1 \times 10^{-4}(\epsilon - 90)^{1.2}}{1 + (\epsilon/8000)^{1.5}} + \frac{7 \times 10^{-5}(\epsilon - 32)^{1.2}}{(1 + \epsilon/2800)^{1.5}}. \quad (3)$$

For 'clean' surfaces formulas, B10 and B12 in [11] are used:

$$\gamma_i(\epsilon) = 0.07 + 1 \times 10^{-5}(\epsilon - 500)^{1.2}/[1 + (\epsilon/70000)^{0.7}], \quad (4)$$

$$\gamma_a(\epsilon) = 1 \times 10^{-5}(\epsilon - 500)^{1.2}/[1 + (\epsilon/70000)^{0.7}]. \quad (5)$$

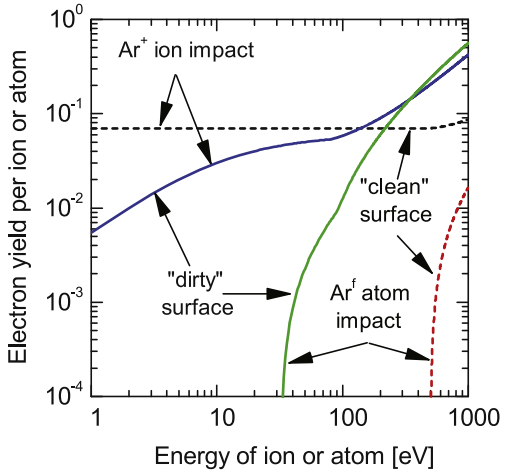

Figure 1. Secondary-electron yields due to Ar^+ and fast Ar atom (Ar^f) impact as a function of the incident particle energy for 'dirty' and 'clean' metal surfaces, calculated based on [11, 48]. Adapted from [11]. © IOP Publishing Ltd. All rights reserved.

The secondary electron yields for argon ion and atom impact as a function of the incident particle energy (ϵ), obtained based on the above formulas, are plotted in figure 1.

In the simulations where an effective SEEC, γ^*, is used, electrons, ions and fast neutrals are traced. In the simulations where we assume a constant SEEC, only electrons and ions are traced, as it is typically done in PIC/MCC simulations of CCPs. The cross sections for electron-neutral and ion-neutral collision processes are taken from [59–61]. For Ar^++ Ar and Ar^f+ Ar collisions, the cross sections are taken from [59]. A detailed description of the model can be found in [17].

Simulations are performed for single-frequency discharges and classical dual-frequency discharges (driven at substantially different frequencies). In single-frequency discharges a voltage waveform of $V(t) = V_0 \cos(2\pi f t)$ with $f = 13.56$ MHz is applied to one electrode located at $x = 0$ cm, while the other electrode at $x = 2.5$ cm is grounded. The neutral gas pressure is varied between 10 and 130 Pa for three different voltage amplitudes (250, 275, and 300 V). In case of dual-frequency excitation the gas pressure is fixed at 6.6 Pa and the driving voltage waveform is: $V(t) = V_{HF} \cos(2\pi f_{HF} t) + V_{LF} \cos(2\pi f_{LF} t)$ with $f_{HF} = 27.12$ MHz and $f_{LF} = f_{HF}/14 \cong 1.937$ MHz. The high-frequency voltage amplitude, V_{HF}, is kept constant at 200 V, and the low-frequency voltage amplitude, V_{LF}, is varied between 0 and 685 V (above this voltage the number of superparticles diverges in the simulations for 'dirty' surfaces due to high values of γ^*). These conditions are chosen to resemble those previously studied based on the assumption of constant ion induced SEECs in [33, 34].

For both single- and dual-frequency discharges, simulations are performed by assuming 'dirty' as well as 'clean' metal electrodes and calculating the effective SEEC self-consistently. The results are compared to those obtained by using a constant SEEC of 0.1 in the simulations. In single-frequency discharges the electron power absorption and ionization dynamics defining the discharge operation mode are investigated, while in dual-frequency discharges the quality of the separate control of ion properties at the electrodes under different surface conditions is also studied.

3. Results

3.1. Single frequency CCPs

Figure 2 shows the spatio-temporal distributions of the ionization rate obtained at three different pressures (at 10, 70, and 130 Pa in panels (a)–(c), respectively) in a single-frequency CCP operated at $f = 13.56$ MHz, $V_0 = 275$ V, and $d = 2.5$ cm. In the simulations a constant SEEC, $\gamma = 0.1$, is assumed for ions, and fast neutrals are not included. The sheath edge positions (shown as white lines in the plots at both electrodes) are calculated based on the criterion proposed by Brinkmann [62]. By increasing the pressure and keeping the voltage amplitude, V_0, constant at 275 V, a transition of the discharge operation mode from the α- to the γ-mode can be observed. At 10 Pa the discharge operates in the α-mode (i.e., the ionization is dominated by electrons heated by sheath expansion, figure 2(a)). Under these conditions one maximum in the ionization rate can be found adjacent to each electrode. As we assume a non-zero SEEC in the simulations ($\gamma = 0.1$), secondary electrons are created upon ion impact at the electrodes, but their collisional multiplication is inefficient at this low pressure. Therefore, they do not induce significant ionization. By increasing the pressure to 70 Pa, these secondary electrons are efficiently multiplied within the sheaths, and the ionization due to these electrons at the time of maximum local sheath voltage becomes comparable to that generated by electrons accelerated by the expanding sheath. At this pressure two distinct maxima of the ionization rate can be observed adjacent to each electrode within one RF period, one at the time of sheath expansion (corresponding to the α-mode and called 'α-peak' hereafter) and another at the time of maximum local sheath voltage (corresponding to the γ-mode and called 'γ-peak' hereafter). The discharge operates in a hybrid α–γ mode (figure 2(b)). A further increase of the pressure leads to strong ionization induced by γ-electrons in the sheath, which is the dominant ionization mechanism at 130 Pa, where the discharge operates in the γ-mode (figure 2(c)).

In figure 2 regions of interest (ROI) around the maxima of the ionization rate (i.e., the α- and γ-peaks), are marked by rectangles at the grounded electrode. These ROIs are used to calculate the averaged intensities of the ionization peaks caused by the α- and γ-modes, I_α and I_γ, respectively. The widths of these regions are determined by finding the times, when the intensity decays to 80% of the peaks. The same procedure is applied to find the height of these regions (i.e., the position where the intensity decays to 80% of the peaks is determined). The results are insensitive to the way the ROIs are determined, confirming the observations of [45]. I_α and I_γ are determined in order to quantify the mode of operation and the transition point from the α- to the γ-mode defined as $I_\gamma/I_\alpha = 1$.

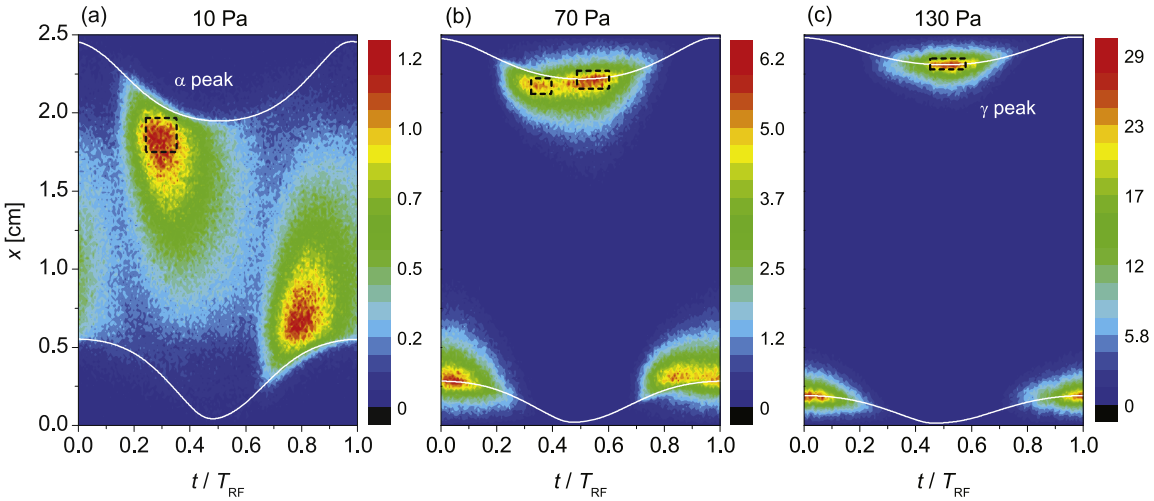

Figure 2. Spatio-temporal plots of the ionization rate obtained by assuming a constant SEEC, $\gamma = 0.1$, in PIC/MCC simulations of single-frequency CCPs at different pressures: (a) 10, (b) 70, and (c) 130 Pa. The rectangles indicate the regions of interest (ROI) around the ionization maxima. The white lines mark the sheath edges adjacent to each electrode. Discharge conditions: $f = 13.56$ MHz, $V_0 = 275$ V, $d = 2.5$ cm. The color scales are given in units of 10^{21} m^{-3} s^{-1}.

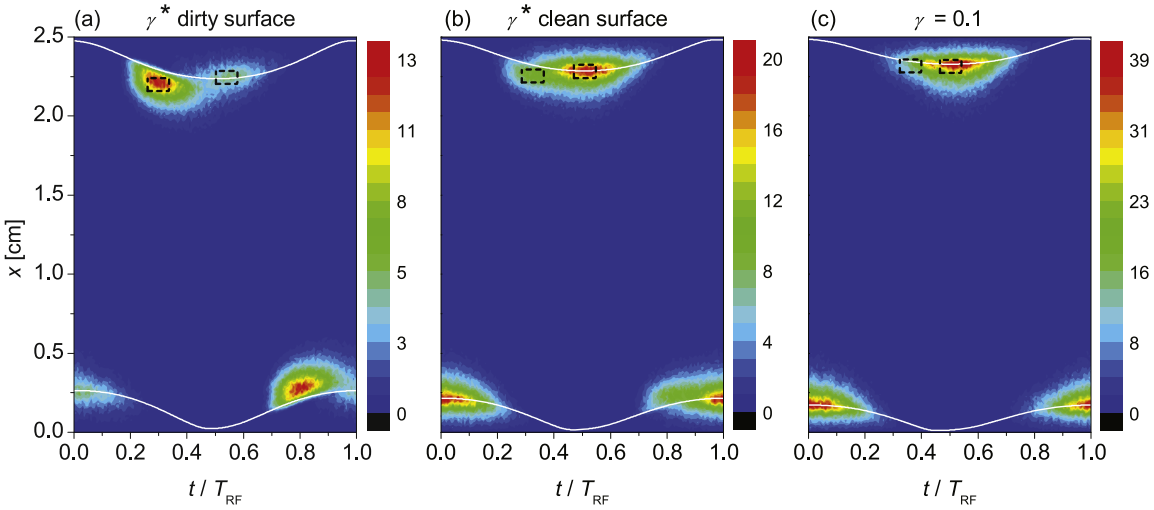

Figure 3. Spatio-temporal plots of the ionization rate obtained from PIC/MCC simulations by using a self-consistently calculated effective SEEC, γ^*, and assuming (a) 'dirty' and (b) 'clean' surface conditions, as well as (c) a constant SEEC, $\gamma = 0.1$. The rectangles indicate the regions of interest (ROI) around the ionization maxima. The white lines mark the sheath edges adjacent to each electrode. Discharge conditions: $p = 130$ Pa, $f = 13.56$ MHz, $V_0 = 300$ V, $d = 2.5$ cm. The color scales are given in units of 10^{21} m^{-3} s^{-1}.

Figure 3 reveals the strong sensitivity of the electron power absorption and ionization dynamics to the surface conditions. The plots show the spatio-temporal distributions of the ionization rate and sheath widths at both electrodes obtained at 130 Pa by using effective SEECs, γ^*, for different surface conditions ('dirty' and 'clean' metal electrodes) in the simulations, as well as using a constant SEEC, $\gamma = 0.1$. The driving voltage amplitude is $V_0 = 300$ V. In case of 'dirty' surface conditions (figure 3(a)), strong ionization due to sheath expansion heating can be observed (α-peak). Weak ionization patterns caused by secondary electrons can also be observed near the sheath boundaries (γ-peak). The discharge operates in the α-mode. Under these conditions, the self-consistently calculated SEEC is $\gamma^* = 0.023$. When 'clean' surface conditions are assumed in the simulation, significant ionization due to both sheath expansion heating and secondary electrons is generated (figure 3(b)) and the discharge operates in a hybrid α–γ mode with ionization mainly due to the γ-mechanism. We find $\gamma^* = 0.07$ under these conditions. Assuming a constant SEEC of $\gamma = 0.1$ in the simulations (figure 3(c)), the discharge operates in the γ-mode (i.e., the γ-peak is dominant).

The transition between the α and the γ electron power absorption modes is described quantitatively by the intensity ratio I_γ/I_α. In figure 4 this ratio is plotted as a function of the neutral gas pressure at $V_0 = 250$ V (figure 4(a)) and $V_0 = 300$ V (figure 4(b)). These plots show the I_γ/I_α ratios obtained by using effective SEECs, γ^*, for 'dirty' and 'clean'

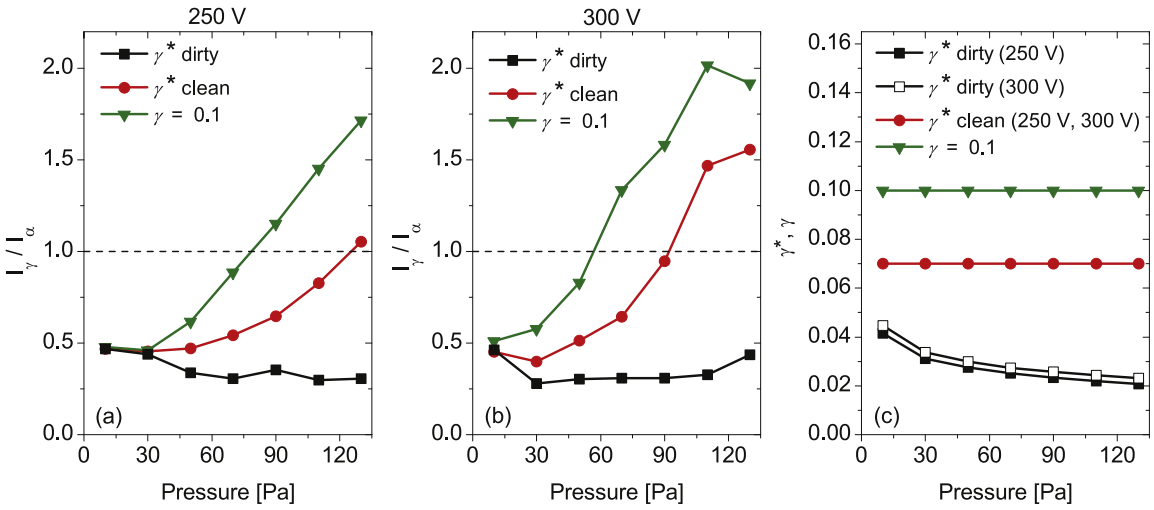

Figure 4. Ratio of the averaged intensities of the maxima caused by secondary electrons, I_γ, and by sheath expansion heating, I_α, obtained from PIC/MCC simulations at (a) $V_0 = 250$ V and (b) $V_0 = 300$ V, by using effective SEECs, γ^*, for 'dirty' and 'clean' metal surfaces, and a constant SEEC, $\gamma = 0.1$, as the pressure is varied. In (c) the SEECs corresponding to these discharge conditions are plotted as a function of pressure. The horizontal dashed lines in (a) and (b) indicate the mode transition characterized by $I_\gamma/I_\alpha = 1$. Discharge conditions: $f = 13.56$ MHz, $d = 2.5$ cm.

surface conditions, as well as $\gamma = 0.1$ in the simulations. In figure 4(c), the SEECs corresponding to these conditions are shown as a function of pressure. At a given pressure, there are significant differences in the I_γ/I_α ratios obtained for the different implementations of the surface conditions characterized by the SEEC in the simulations, especially at high pressures.

At $V_0 = 250$ V, assuming $\gamma = 0.1$ in the simulations, the I_γ/I_α ratio increases by a factor of about 3.5 as the pressure is increased from 10 to 130 Pa (figure 4(a)). The transition between the α- and γ-modes takes place at about 78 Pa, where $I_\gamma/I_\alpha = 1$. Above this pressure the I_γ/I_α ratio is higher than 1. This can be explained by the effect of the secondary electrons on the ionization dynamics at different pressures. By increasing the pressure, the collisional multiplication of secondary electrons (emitted with a probability of 0.1 as a result of ion impact at the electrodes) becomes more efficient in the sheaths, which leads to ionization dominated by γ-electron avalanches at high pressures. Therefore, higher values for I_γ and higher values for the I_γ/I_α ratios are observed. Assuming 'clean' surface conditions in the simulations, the I_γ/I_α ratio increases as the pressure is increased, analogous to the scenario seen at $\gamma = 0.1$. In this case, however, the I_γ/I_α ratio changes by only a factor of 2.25 by increasing the pressure from 10 to 130 Pa, and slightly exceeds one only at the highest pressure investigated. This can be explained by the low values of γ^* (lower than 0.1) calculated in the simulations self-consistently (figure 4(c)): γ^* is 0.07 at all pressures investigated for 'clean' metal surfaces, because for particle energies below 500 eV fast neutrals do not induce secondary electrons and the ion induced secondary electron yield is 0.07 per ion impact (see figure 1). Under the conditions studied here, the ion energies are well below 500 eV, as are the energies of the fast neutrals. Therefore, only ions contribute to secondary electron emission, which explains the constant low value of γ^* at all pressures [11]. Compared to the case of $\gamma = 0.1$, the transition from the α- to the γ-mode takes place at higher pressure for 'clean' metal electrodes. Assuming 'dirty' surface conditions in the simulations, a slight decrease of the I_γ/I_α ratio is found as the pressure is changed from 10 to 130 Pa. The I_γ/I_α ratio is below 0.5 for all pressures. Therefore, the discharge operation mode is not changed by varying the pressure under these conditions and the discharge operates in the α-mode at all pressures. γ^* is below 0.04 and slightly decreases by increasing the pressure. At the same time, the mean energy of the heavy particles decreases because the sheaths are more collisional at high pressures. This leads to a decrease of the energy-dependent secondary electron yield upon heavy particle impact and to a decrease of the effective SEEC, γ^*, for 'dirty' surfaces (figure 4(c)).

An increase of the driving voltage amplitude by 50 V, from $V_0 = 250$ V to $V_0 = 300$ V, leads to a remarkable decrease of the pressure value at which the transition between the α- and the γ-mode takes place (figure 4(b)). This can be explained by the enhancement of the γ ionization peak at higher voltage amplitudes.

In figure 5 the ion density at the center of the discharge, the ion flux, Γ_i, and the mean energy of ions reaching the electrodes, $\langle E_i \rangle$, are shown as a function of the gas pressure for $V_0 = 300$ V, obtained by using effective SEECs, γ^*, for 'dirty' and 'clean' surface conditions, as well as $\gamma = 0.1$. For $\gamma = 0.1$, the plasma density increases by a factor of about 6.3 by increasing the pressure from 10 to 130 Pa, the highest plasma density is $6.25 \times 10^{16}\,\mathrm{m}^{-3}$ at 130 Pa (figure 5(a)). The increase of the plasma density as well as the increase of the ion flux at the electrodes (figure 5(b)) with increasing pressure can be explained by the more efficient multiplication of secondary electrons at higher pressures due to the decrease of the mean free path of electrons. Much lower values for the plasma density and ion flux are obtained when realistic

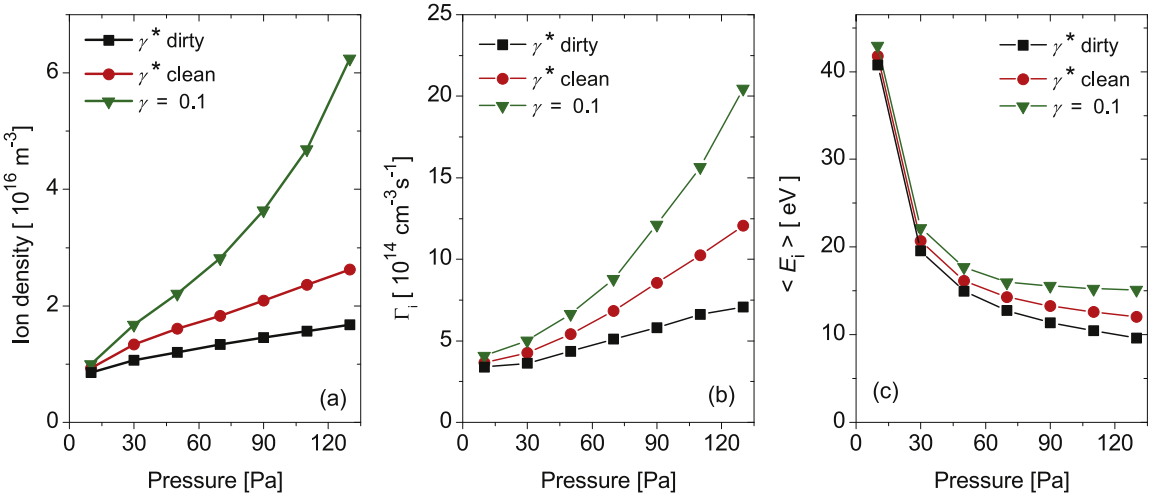

Figure 5. PIC/MCC simulation results for (a) the ion density in the center of the discharge, (b) the ion flux, Γ_i, and (c) the mean ion energy, $\langle E_i \rangle$, at the electrodes as a function of the gas pressure obtained by using effective SEECs, γ^*, for 'dirty' and 'clean' surfaces, and a constant SEEC, $\gamma = 0.1$. Discharge conditions: $f = 13.56$ MHz, $V_0 = 300$ V, $d = 2.5$ cm.

SEECs are used in the simulations for different surface conditions. The maximum plasma density is $2.6 \times 10^{16}\,\mathrm{m}^{-3}$ for 'clean' surfaces and $1.7 \times 10^{16}\,\mathrm{m}^{-3}$ for 'dirty' surfaces. The lower plasma densities obtained by using effective secondary electron emission yields for heavy particles compared to the case of $\gamma = 0.1$ can be explained by the low values of γ^* obtained from the simulations (see figure 4(c)) and their effects on the spatio-temporal ionization dynamics: γ^* is 0.07 for 'clean' surfaces at all pressures, while its value drops below 0.05 for 'dirty' surfaces. At a given pressure and voltage amplitude, low values of the SEEC result in the generation of fewer secondary electrons at the electrodes. Therefore, less ionization due to electron avalanches induced by secondary electrons in the sheath and lower plasma densities are found. At lower plasma densities the sheath width is larger, the ions undergo more collisions inside the sheaths and arrive at the electrodes at lower energies compared to the case of $\gamma = 0.1$ (figure 5(c)). This is a self-amplifying mechanism for 'dirty' metal surfaces that leads to even lower values of γ^*.

In conclusion, we found that the pressure at which the transition between the α- and γ-mode of the electron power absorption is observed depends strongly on the surface conditions. Compared to the case of $\gamma = 0.1$, the transition from the α- to the γ-mode takes place at higher pressure when realistic energy-dependent secondary electron yields for heavy particles on 'clean' electrode surfaces are used in the simulations. By increasing the driving voltage amplitude, this transition is shifted towards lower pressures. For 'dirty' metal surfaces, the discharge operates in the α-mode for all conditions investigated. Lower values for the plasma density and the ion flux at the electrodes are obtained when realistic SEECs are used in the simulations. The difference between the results obtained by using γ^* and constant $\gamma = 0.1$ in the simulations can be explained by the low values of γ^* obtained from the simulations. γ^* is 0.07 for 'clean' metal surfaces at all conditions investigated, while it takes values below 0.05 for 'dirty' metal surfaces. The self-consistently calculated γ^* values are smaller than 0.1 for all conditions investigated here. Therefore, in simulations with constant $\gamma = 0.1$ the importance of the secondary electron emission process is overestimated under the discharge conditions studied here. Including realistic γ-coefficients in PIC/MCC simulations of CCPs is crucially important to obtain realistic results.

3.2. Dual frequency CCPs

The effect of the surface conditions on the ionization dynamics and the separate control of the mean ion energy, $\langle E_i \rangle$, and ion flux, Γ_i, at the electrodes is studied for a classical dual-frequency discharge in argon for a gap distance of 2.5 cm. The driving frequencies are $f_{HF} = 27.12$ MHz and $f_{LF} = 1.937$ MHz. The high-frequency voltage amplitude is held constant at $V_{HF} = 200$ V. The low-frequency voltage amplitude, V_{LF}, which is the control parameter for the mean ion energy, is varied from 0 to 685 V at 6.6 Pa. The choice of these discharge conditions is motivated by previous studies performed at similar discharge conditions in order to clarify the effect of secondary electrons on the ionization dynamics and on the quality of the separate control of ion properties at the electrodes in classical dual-frequency discharges [33, 34]. In these previous studies different (constant) secondary electron yields were used for ions in PIC/MCC simulations and different behaviors of the ion flux as a function of V_{LF} were obtained depending on the choice of γ: for low values of γ, the ion flux was found to decrease as a function of V_{LF}, a nearly constant ion flux independent of V_{LF} was obtained for $0.1 \leqslant \gamma \leqslant 0.15$, while for high γ coefficients the ion flux was found to increase as a function of V_{LF}.

Figure 6 shows the flux and the mean energy of ions at the electrodes, Γ_i and $\langle E_i \rangle$, respectively, as a function of the low-frequency voltage amplitude, V_{LF}, obtained for different surface conditions by assuming 'dirty' and 'clean' metal electrodes in the simulations (panels (a) and (b)), with the

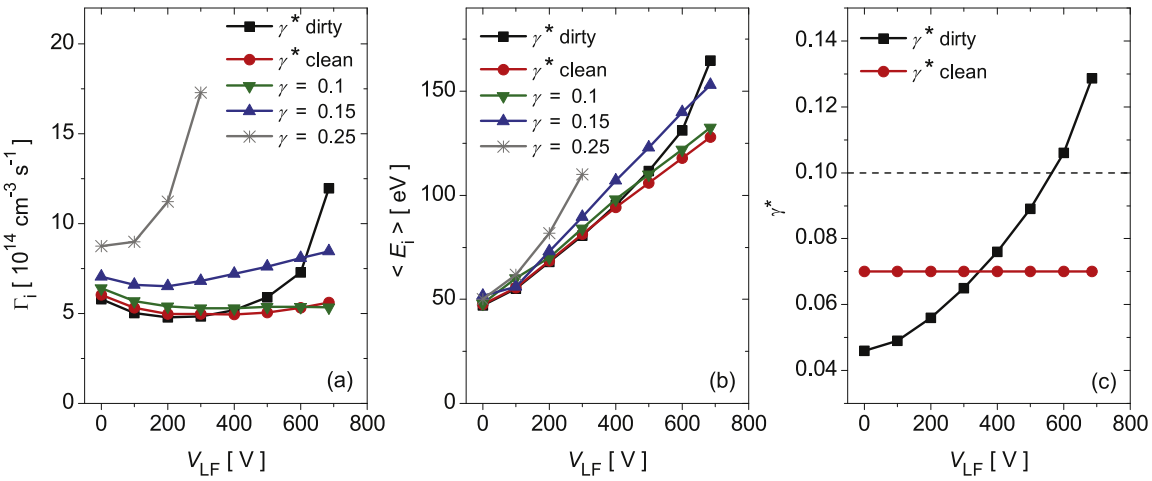

Figure 6. (a) Ion flux, Γ_i, and (b) mean ion energy, $\langle E_i \rangle$, at the electrodes as a function of the low-frequency voltage amplitude, obtained from PIC/MCC simulations by using effective SEECs, γ^*, for 'dirty' and 'clean' metal surfaces, and a constant ion induced SEECs ($\gamma = 0.1$, 0.15, and 0.25). The effective SEECs are plotted in panel (c). The horizontal dashed line in (c) indicates the constant ion induced SEEC $\gamma = 0.1$. Discharge conditions: $p = 6.6$ Pa, $f_{HF} = 27.12$ MHz, $V_{HF} = 200$ V, $f_{LF} = 1.973$ MHz, $d = 2.5$ cm.

effective γ^* SEECs calculated self-consistently in the simulations based on equation (1) (panel (c)). The mean ion energies as well as the ion fluxes are identical at both electrodes due to the symmetry of the discharge. In panels (a) and (b) of figure 6 results for Γ_i and $\langle E_i \rangle$ obtained by using constant SEECs are also included: values of 0.1, 0.15 and 0.25 are set for γ to illustrate the decreasing, nearly constant, as well as the increasing trends observed in [33, 34] for the ion flux at the electrodes as a function of V_{LF}. In these simulations with constant SEECs electrons and ions are traced and the inelastic ion-neutral collision processes are neglected, in accordance with the simulations in [33, 34].

Important differences from the results obtained previously for constant SEECs [33, 34] are found for the ion flux as a function of V_{LF} if realistic self-consistently calculated effective SEECs are used in the simulations for 'dirty' metal surfaces, since γ^* changes as a function of V_{LF} due to the corresponding change of $\langle E_i \rangle$. At $V_{LF} < 200$ V, the ion flux decreases by increasing V_{LF}. This is caused by the effect known as frequency coupling in classical dual-frequency discharges [63–66]. Under these conditions the discharge operates in the α-mode for $V_{LF} = 0$ V (figure 8, first row). By increasing the low-frequency voltage amplitude, the oscillating sheath edge is pushed away from the electrode during a significant fraction of the low-frequency period into a region characterized by a higher plasma density (figure 8, second and third rows), which reduces the sheath expansion velocity and the ionization caused by energetic electrons in this region. This effect leads to a decrease of the ion flux as a function of V_{LF}. At $V_{LF} < 200$V, the effective γ^* increases with V_{LF}, but it remains low (below 0.06) and the ionization induced by secondary electrons is not significant under these conditions. By increasing the low-frequency voltage amplitude, the contribution of fast atoms to the emission of secondary electrons is enhanced (figure 7(a)). At 200 V $< V_{LF} <$ 400 V the ion flux is nearly constant, while γ^* increases from 0.056 to 0.076. Under these conditions the ionization induced by secondary electron avalanches becomes significant (see figure 8, second row) and the negative effect of the frequency coupling on the ionization (decrease of the ion flux) is compensated by the influence of γ-electrons (increase of the ion flux). At increased low-frequency voltage amplitudes ($V_{LF} > 400$ V) the ion flux increases rapidly: Γ_i changes by a factor of 2.3 by increasing V_{LF} from 400 to 685 V. This can be explained by the increase of γ^* with V_{LF} due to the higher heavy particle energies at the electrodes (figures 7(b) and (c)). The value of γ^* becomes larger than 0.1 at about 560 V and reaches the maximum value of 0.13 at $V_{LF} = 685$ V, where about 40% of the secondary electrons are generated by fast neutral impact at the electrodes (figure 7(a)). For high values of the SEEC, the increasing low-frequency voltage amplitude leads to a strong increase of the ionization generated by secondary electrons, and, therefore, Γ_i increases with V_{LF} (figure 8, third row). We note that at $V_{LF} = 685$ V, the ion flux at the electrodes obtained for 'dirty' surface conditions based on simulations, where ions and fast neutrals are traced, is higher than that obtained by assuming a constant ion-induced SEEC of $\gamma = 0.15$ in simulations where only ions are traced. This happens despite the fact that the self-consistently calculated effective SEEC $\gamma^* = 0.13 < 0.15$. This indicates the important role of fast neutrals and heavy-particle processes in the discharge under the conditions studied here.

In figure 8 the contributions of electrons, ions, and fast neutrals to the total ionization rate (shown in figure 9(a)) are presented for different values of V_{LF} (0, 300, and 685 V) for 'dirty' surface conditions. Most of the ionization is generated by electrons for all values of V_{LF} (figure 8, first column). Close to the electrodes, ionization is induced by heavy particles as well. The ionization rates due to ions and fast neutrals are on the same order of magnitude (figure 8, second and third columns). The ionization by heavy particles becomes significant at the electrodes at higher values of the low-frequency voltage amplitude. If the ion transit time through the sheath is comparable to the low-frequency period, the heavy

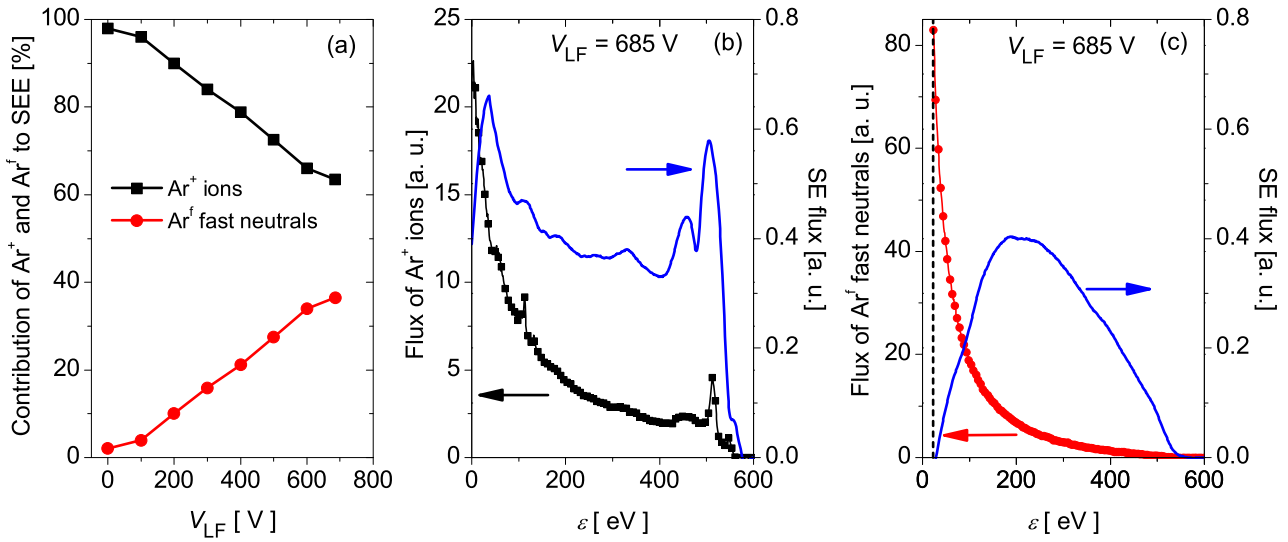

Figure 7. (a) The contribution of ions and fast atoms to the secondary electron emission as a function of the low-frequency voltage amplitude obtained from PIC/MCC simulations by using effective SEECs, γ^*, for 'dirty' metal surfaces. The flux energy distributions of ions (b) and fast atoms (c) at the electrodes (left vertical axis) and the secondary electron flux induced by these particles (right vertical axis) as a function of the ion/atom energy for $V_{LF} = 685$ V, 'dirty' metal surfaces. The dashed vertical line in (c) indicates the threshold energy of 23 eV for fast atoms. Discharge conditions: $p = 6.6$ Pa, $f_{HF} = 27.12$ MHz, $V_{HF} = 200$ V, $f_{LF} = 1.973$ MHz, $d = 2.5$ cm.

particle induced ionization is time modulated. It has a maximum shortly after the time of maximum sheath voltage at each electrode, when the ions have been accelerated to high velocities. In this way electrons are generated inside the sheath shortly after the time of maximum absolute local sheath voltage. For the same reason, the number of secondary electrons is maximized shortly after the time of maximum absolute local sheath voltages at both electrodes. These electrons, which are induced by heavy particle impact ionizations and secondary electron emission, are accelerated towards the plasma bulk and induce electron avalanches, which further enhance the ionization. This causes a maximum of the electron induced ionization shortly after the time of maximum sheath expansion (figure 8, bottom left). The effect is especially pronounced at $V_{LF} = 685$ V.

For 'clean' metal surfaces, the results are similar to those obtained for 'dirty' electrodes, but for high values of the low-frequency voltage amplitude ($V_{LF} > 500$ V), Γ_i changes only slightly with increasing V_{LF} (figure 6(a)) and γ^* remains constant at 0.07 independent of V_{LF} (figure 6(c)). Due to this low (constant) value of γ^*, less secondary electrons are generated at the electrodes, which have a moderate effect on the ionization (figure 9(b)).

The mean ion energy can be efficiently controlled by V_{LF} (figure 6(b)). For all constant values of γ, as well as in case of using γ^* SEECs for different surface conditions, $\langle E_i \rangle$ increases as a function of V_{LF} due to the increase of the mean sheath voltage.

Figure 9 shows the total ionization rate induced by all particles traced in the simulation obtained by using the effective SEECs for 'dirty' and 'clean' metal surfaces, and a constant $\gamma = 0.1$, for the highest low-frequency voltage amplitude of $V_{LF} = 685$ V. Compared to the case of $\gamma = 0.1$ (panel (c)), additional ionization can be observed in the sheath region when energy-dependent secondary electron yields for heavy particles are implemented in the simulations (panels (b) and (c)), especially for 'dirty' surface conditions (see also figure 8, third row).

In conclusion, we found that the surface conditions affect the quality of the separate control of ion properties at the electrodes in classical dual-frequency discharges. By assuming 'dirty' metal surfaces in the simulations, the self-consistently calculated effective SEEC γ^* increases with V_{LF}. This variation of γ^* as a function of V_{LF} results in a decrease of the ion flux at low values of V_{LF} and a strong increase of Γ_i at high low-frequency voltage amplitudes. The separate control of ion properties can be attained only in a narrow process window, where the negative effect of the frequency coupling on the ionization is compensated by the ionization induced by γ-electrons. Such a scenario was found by assuming 'clean' metal surfaces in the simulations. In this case γ^* does not change, it has a low value of 0.07 under the conditions studied here. Therefore, Γ_i changes only slightly by changing the low-frequency voltage amplitude. The new results on the separate control of ion properties in classical dual-frequency discharges obtained by using self-consistently calculated effective SEECs in the simulations and assuming 'dirty' surface conditions are different from previous simulation results obtained with constant values of γ [33, 34]. The new results show that the self-consistent calculation of the SEEC has a strong influence on the discharge characteristics. For the highest value of the low-frequency voltage amplitude ($V_{LF} = 685$ V) studied here $\gamma^* = 0.13$ based on simulations, where ions and fast neutrals are traced. However, the flux of ions to the electrodes obtained in this case is higher by about 40% than the flux of ions obtained for the constant ion-induced SEEC of $\gamma = 0.15$ in simulations, where only ions are traced. This reflects that the effect of fast neutrals and that

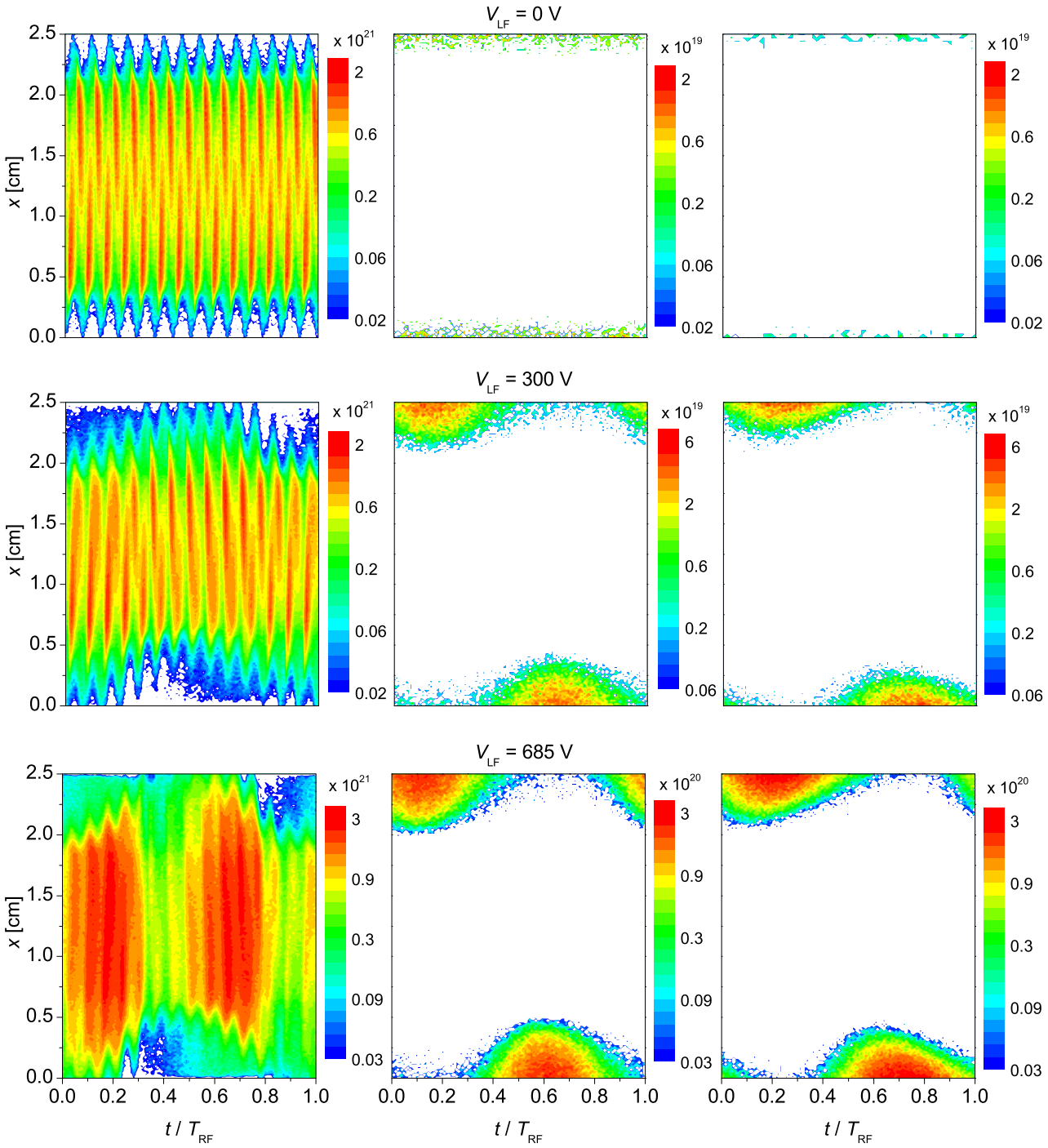

Figure 8. Spatio-temporal plot of the contributions of electrons (first column), ions (second column), and fast neutrals (third column) to the total ionization obtained from PIC/MCC simulations by using an effective SEEC, γ^*, and assuming 'dirty' surface conditions at $V_{LF} = 0$ V (first row), $V_{LF} = 300$ V (second row), and $V_{LF} = 685$ V (third row). Discharge conditions: $p = 6.6$ Pa, $f_{HF} = 27.12$ MHz, $V_{HF} = 200$ V, $f_{LF} = 1.973$ MHz, $d = 2.5$ cm. The color scales are logarithmic, cover two orders of magnitude and are given in units of m^{-3} s^{-1}.

of heavy-particle dynamics on the calculated discharge characteristics are significant and must be taken into account in PIC/MCC simulations in order to obtain a realistic description of CCPs.

4. Conclusions

We have studied the effects of using realistic energy-dependent SEECs and taking into account the properties of the electrode surfaces on the calculated plasma parameters in PIC/MCC simulations of low-pressure CCPs in argon. We

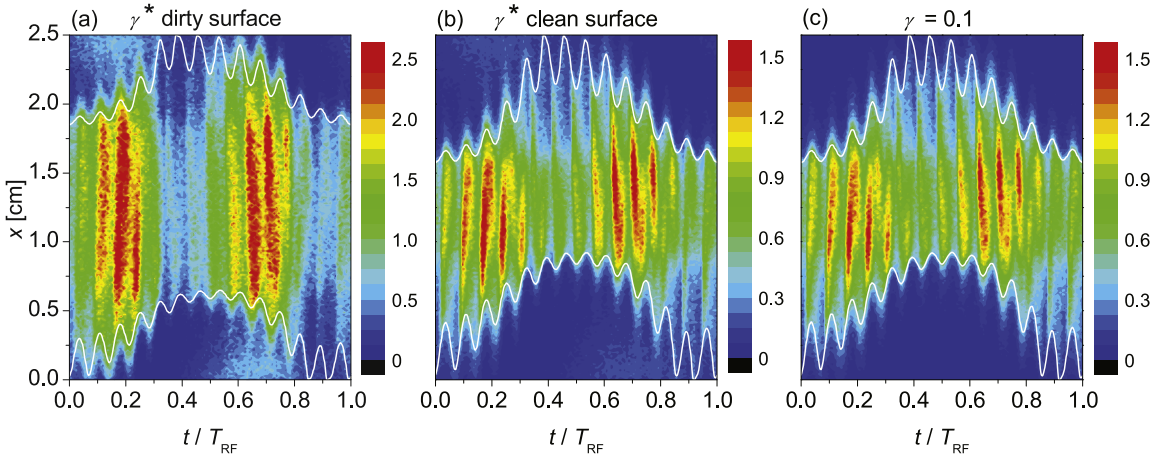

Figure 9. Spatio-temporal plots of the ionization rate obtained from PIC/MCC simulations by using an effective SEEC, γ^*, and assuming (a) 'dirty' and (b) 'clean' surface conditions, and (c) using a constant ion induced SEEC, $\gamma = 0.1$. The white lines mark the sheath edges adjacent to each electrode. Discharge conditions: $p = 6.6$ Pa, $f_{HF} = 27.12$ MHz, $V_{HF} = 200$ V, $f_{LF} = 1.973$ MHz, $V_{LF} = 685$ V, $d = 2.5$ cm. The color scales are given in units of 10^{21} m^{-3} s^{-1}.

have performed simulations using energy-dependent SEECs for 'clean' and 'dirty' metal surfaces in single- and dual-frequency discharges, and compared the results to those obtained by assuming a constant secondary electron yield of $\gamma = 0.1$ for ions.

In single-frequency discharges (13.56 MHz), simulations were performed at different pressures between 10 and 130 Pa for three different voltage amplitudes and the transition of the discharge operation mode between the α-mode and the γ-mode was studied. We found that the pressure and voltage at which the transition between these modes is observed strongly depends on the surface conditions: for 'clean' metal surfaces the transition takes place at a higher pressure compared to the case of $\gamma = 0.1$, while for 'dirty' metal surfaces, the discharge operates in α-mode for all conditions investigated. Lower values for the plasma density and ion flux at the electrodes are obtained when realistic SEECs are used in the simulations. The source of these disagreements is the difference in the value of γ^* obtained by assuming realistic surface conditions, which differ from 0.1: γ^* is 0.07 for 'clean' metal surfaces at all conditions investigated, while it takes values below 0.05 for 'dirty' metal surfaces. We note that under the conditions investigated here the heavy particle energies at the electrodes are low compared to operating conditions of e.g. sputtering or plasma immersion ion implantation applications. Therefore, 'dirty' (oxidized) surfaces have a lower effective SEEC, γ^*, compared to 'clean' metal surfaces. For higher voltages higher heavy particle energies can be reached, which result in γ^* for 'dirty' surfaces to be higher than γ^* for 'clean' metal electrodes. Therefore, the results are expected to be reversed at high heavy particle energies, i.e., higher plasma densities and ion fluxes at the electrodes are expected to be obtained for 'dirty' surfaces compared to 'clean' metal electrodes.

In classical dual-frequency discharges (27.12 MHz + 1.937 MHz), simulations were performed at 6.6 Pa for different values of the low-frequency voltage amplitude and the ionization dynamics as well as the separate control of the mean ion energy and ion flux at the electrodes were analyzed for different surface conditions. For 'dirty' metal surfaces, we have found differences from previous results on the separate control of ion properties in classical dual-frequency discharges obtained with different constant values of γ under similar discharge conditions. The reason for this is that the effective SEEC, γ^*, changes by varying the control parameter for the mean ion energy. We note that our study is restricted to relatively low heavy particle energies. For 'dirty' metal surfaces, γ^* significantly increases by increasing the low-frequency voltage amplitude, V_{LF}. At the highest value of the low-frequency voltage amplitude ($V_{LF} = 685$ V) applied here, γ^* reaches the maximum value of 0.13 and is higher than γ^* for 'clean' metal electrodes. The flux of ions to the electrodes obtained in this case is higher than the flux of ions obtained for the constant ion-induced SEEC of $\gamma = 0.15$, which indicates the importance of taking into account fast neutrals in PIC/MCC simulations of CCPs. The separate control of ion properties can be attained only in a narrow process window, where the negative effect of the frequency coupling on the ionization is compensated by the ionization induced by γ-electrons. At high values of V_{LF}, heavy particles can also induce significant ionization. In order to obtain realistic results from PIC/MCC simulations of low-pressure CCPs, the precise description of the secondary electron emission process via realistic γ-coefficients is very important.

In this study, the realistic values of the SEECs were calculated based on formulas provided for argon ions and atoms for 'clean' and 'dirty' metal electrodes. Therefore, the above conclusions are primarily valid for argon discharges. In case of other gases, the energy-dependent secondary electron yields due to heavy particle impact for different surface conditions can be different from the ones obtained for argon, which could significantly affect the calculated discharge characteristics.

Acknowledgments

This work was supported by the US NSF grant no. 1601080, by the German Research Foundation (DFG) within the frame of the collaborative research centre SFB-TR 87, and by the Hungarian National Research, Development and Innovation Office (NRDI Office) via grants K-119357 and PD-121033.

References

[1] Lieberman M A and Lichtenberg A J 2005 *Principles of Plasma Discharges and Materials Processing* 2nd edn (New York: Wiley)
[2] Makabe T and Petrović Z 2006 *Plasma Electronics: Applications in Microelectronic Device Fabrication* (London: Taylor and Francis)
[3] Chabert P and Braithwaite N 2011 *Physics of Radio-Frequency Plasmas* (Cambridge: Cambridge University Press)
[4] Birdsall C K and Langdon A B 1985 *Plasma Physics via Computer Simulation* (New York: McGraw-Hill)
[5] Hockney R W and Eastwood J W 1981 *Computer Simulation Using Particles* (New York: McGraw-Hill)
[6] Birdsall C K 1991 *IEEE Trans. Plasma Sci.* **19** 65
[7] Diomede P, Capitelli M and Longo S 2005 *Plasma Sources Sci. Technol.* **14** 459
[8] Matyash K, Schneider R, Taccogna F, Hatazarna A, Longo S, Capitelli M, Tskhakaya D and Bronold F X 2007 *Contrib. Plasma Phys.* **47** 595
[9] Verboncoeur J P 2005 *Plasma Phys. Control. Fusion* **47** A231
[10] Donkó Z 2011 *Plasma Sources Sci. Technol.* **20** 24001
[11] Phelps A V and Petrović Z L 1999 *Plasma Sources Sci. Technol.* **8** R21
[12] Corbella C, Marcak A, de los Arcos T and von Keudell A 2016 *J. Phys. D: Appl. Phys.* **49** 16LT01
[13] Bronold F X and Fehske H 2015 *Phys. Rev. Lett.* **115** 225001
[14] Bronold F X and Fehske H 2017 *Plasma Phys. Control. Fusion* **59** 014011
[15] Hagstrum H D 1954 *Phys. Rev.* **96** 336
[16] Hagstrum H D 1961 *Phys. Rev.* **122** 83
[17] Derzsi A, Korolov I, Schüngel E, Donkó Z and Schulze J 2015 *Plasma Sources Sci. Technol.* **24** 034002
[18] Korolov I, Derzsi A, Donkó Z, Schüngel E and Schulze J 2016 *Plasma Sources Sci. Technol.* **25** 015024
[19] Braginsky O, Kovalev A, Lopaev D, Proshina O, Rakhimova T, Vasilieva A, Voloshin D and Zyryanov S 2012 *J. Phys. D: Appl. Phys.* D **45** 015201
[20] Bojarov A, Radmilović-Radjenović M and Petrović Z L 2010 *Proc. 20th ESCAMPIG (Novi Sad, Serbia, 13–17 July 2010)* p 2.38
Bojarov A, Radmilović-Radjenović M and Petrović Z L 2010 *Publ. Astron. Obs. Belgrade* p 131
Bojarov A, Radmilović-Radjenović M and Petrović Z L 2012 *Proc. 65th Annual Gaseous Electronics Conf. (Austin, Texas, 22–26 October 2012)*
Bojarov A, Radmilović-Radjenović M and Petrović Z L 2014 *Proc. 27th Summer School and Int. Sym. on the Physics of Ionized Gases (Belgrade, Serbia, 26–29 August 2014)*
[21] Radmilović-Radjenović M and Petrović Z L 2009 *Eur. Phys. J.* D **54** 445
[22] Gudmundsson J T, Kawamura E and Lieberman M A 2013 *Plasma Sources Sci. Technol.* **22** 035011
[23] Hannesdottir H and Gudmundsson J T 2016 *Plasma Sources Sci. Technol.* **25** 055002
[24] Greb A, Niemi K, O'Connell D and Gans T 2013 *Appl. Phys. Lett.* **103** 244101
[25] Belenguer P and Boeuf J P 1990 *Phys. Rev.* A **41** 4447
[26] Schulze J, Heil B G, Luggenhölscher D and Czarnetzki U 2008 *IEEE Trans. Plasma Sci.* **36** 1400
[27] Schulze J, Heil B G, Luggenhölscher D, Brinkmann R P and Czarnetzki U 2008 *J. Phys. D: Appl. Phys.* **41** 195212
[28] Schulze J, Kampschulte T, Luggenhölscher D, Brinkmann R P and Czarnetzki U 2008 *J. Phys.: Conf. Ser.* **86** 12010
[29] Turner M M 2009 *J. Phys. D: Appl. Phys.* **42** 194008
[30] Mussenbrock T, Brinkmann R P, Lieberman M A, Lichtenberg A J and Kawamura E 2008 *Phys. Rev. Lett.* **101** 085004
[31] Schweigert V A, Alexandrov A L, Gimelshtein S F and Ivanov M S 1999 *Plasma Sources Sci. Technol.* **8** B1
[32] Ivanov V V, Popov A M and Rakhimova T V 1995 *Plasma Phys. Rep.* **21** 515
[33] Donkó Z, Schulze J, Hartmann P, Korolov I, Czarnetzki U and Schüngel E 2010 *Appl. Phys. Lett.* **97** 081501
[34] Schulze J, Donkó Z, Schüngel E and Czarnetzki U 2011 *Plasma Sources Sci. Technol.* **20** 045007
[35] Turner M M, Chabert P, Levif P, Boyle P and Robiche J 2007 *Proc. 18th ICPIG (Prague, Czech Republic)* p G08
[36] Booth J P, Curley G, Marić D and Chabert P 2010 *Plasma Sources Sci. Technol.* **19** 015005
[37] Böhm C and Perrin J 1993 *Rev. Sci. Instrum.* **64** 31
[38] Liu Q, Liu Y, Samir T and Ma Z 2014 *Phys. Plasmas* **21** 083511
[39] Lafleur T, Chabert P and Booth J P 2013 *J. Phys. D: Appl. Phys.* **46** 135201
[40] Korolov I, Derzsi A, Donkó Z and Schulze J 2013 *Appl. Phys. Lett.* **103** 064102
[41] Czarnetzki U, Heil B G, Schulze J, Donkó Z, Mussenbrock T and Brinkmann R P 2009 *J. Phys.: Conf. Ser.* **162** 012010
[42] Donkó Z 2000 *J. Appl. Phys.* **88** 2226
[43] Donkó Z 2001 *Phys. Rev.* E **64** 026401
[44] Marić D, Hartmann P, Malović G, Donkó Z and Petrović Z L 2003 *J. Phys. D: Appl. Phys.* **36** 2639
[45] Daksha M, Berger B, Schüngel E, Korolov I, Derzsi A, Koepke M, Donkó Z and Schulze J 2016 *J. Phys. D: Appl. Phys.* **49** 234001
[46] Bogaerts A and Gijbels R 1995 *J. Appl. Phys.* **78** 6429
[47] Bogaerts A and Gijbels R 1999 *IEEE Trans. Plasma Sci.* **27** 1406
[48] Phelps A V, Pitchford L C, Pédoussat C and Donkó Z 1999 *Plasma Sources Sci. Technol.* **8** B1–2
[49] Kitajima T, Takeo Y, Petrović Z L and Makabe T 2000 *Appl. Phys. Lett.* **77** 849
[50] Boyle P C, Ellingboe A R and Turner M M 2004 *Plasma Sources Sci. Technol.* **13** 493
[51] Boyle P C, Ellingboe A R and Turner M M 2004 *J. Phys. D: Appl. Phys.* **37** 697
[52] Donkó Z 2011 *Plasma Sources Sci. Technol.* **20** 024001
[53] Donkó Z, Schulze J, Czarnetzki U, Derzsi A, Hartmann P, Korolov I and Schüngel E 2012 *Plasma Phys. Control. Fusion* **54** 124003
[54] Taccogna F and Dilecce G 2016 *Eur. Phys. J.* D **70** 251
[55] Rauf S and Kushner M J 1999 *IEEE Trans. Plasma Sci.* **27** 1329
[56] Lee J K, Babaeva N, Kim H C, Manuilenko O and Shon J W 2004 *IEEE Trans. Plasma Sci.* **32** 47
[57] Lee H-C and Chung C-W 2012 *Appl. Phys. Lett.* **101** 244104
[58] Kollath R 1956 *Encyclopedia of Physics* ed S Flügge vol 21 (Berlin: Springer) p 264
[59] Phelps A V 2005 http://jilawww.colorado.edu/~avp/collision_data/
[60] Phelps A V 1991 *J. Phys. Chem. Ref. Data* **20** 557
[61] Phelps A V 1994 *J. Appl. Phys.* **76** 747
[62] Brinkmann R P 2007 *J. Appl. Phys.* **102** 093303

[63] Turner M M and Chabert P 2006 *Phys. Rev. Lett.* **96** 205001
[64] Gans T, Schulze J, O'Connell D, Czarnetzki U, Faulkner R, Ellingboe A R and Turner M M 2006 *Appl. Phys. Lett.* **89** 261502
[65] Schulze J, Gans T, O'Connell D, Czarnetzki U, Ellingboe A R and Turner M M 2007 *J. Phys. D: Appl. Phys.* **40** 7008
[66] Donkó Z 2007 *Proc. Symp. of Application of Plasma Processes* vol 2 *(Podbanske, Slovakia, 20–25 January 2007)* ed J Matuska *et al* pp 21–4 IL0